

# Control Performance and Stability Analysis of Frequency Estimator in Grid-forming Synchronization Control

Jaume Girona-Badia, Juan Carlos Olives-Camps, Vinicius Albernaz Lacerda, Eduardo Prieto-Araujo, and Oriol Gomis-Bellmunt

**Abstract**—This paper analyzes the effect of a frequency estimator in a grid-forming (GFM) synchronization control on the stability and control performance. GFM control for power converters has been proposed as a promising solution to enhance the stability and resilience of electrical systems dominated by power electronics. However, no consensus has been reached on the control structure for this operation mode. Moreover, the interactions between different GFM schemes and frequency estimators are not completely defined in the literature. In this paper, the effect of adding a frequency estimator to the two main industry-class synchronization controls, i.e., droop and virtual synchronous machine (VSM), is studied. Additionally, different AC voltage measurement points, tuning, and structures of frequency estimator are considered. Two distinct analyses are performed to discuss the characteristics of different configurations: ① an analytical study on the control performance of different configurations, and ② a small-signal analysis to ensure system stability. Finally, the results are validated using dynamic simulations, followed by a discussion. This paper concludes that the droop should be avoided when applying a frequency estimator, and other structures such as the VSM are more desirable.

**Index Terms**—Droop, virtual synchronous machine (VSM), frequency estimator, grid-forming (GFM), synchronization control, stability analysis.

## I. INTRODUCTION

THE penetration of renewable energy sources into the AC network has increased over the last decades as an outcome of climate concerns [1]. As a consequence, a significant percentage of power that used to be supplied by synchronous generator (SG)-based power plants is being supplied by inverter-based resources (IBRs). Power networks

dominated by IBRs might experience reduced strength [2]. Under such conditions, the grid-forming (GFM) control strategy is one of the most promising solutions to increase the AC network stability [3], [4]. This control strategy can be applied to the grid-connected converters such as energy-storage static synchronous compensators (E-STATCOMs), high-voltage direct current (HVDC) converters, and inverter-based resource (IBR). The grid support that converters can provide will depend on their specific capabilities.

Although the general parameters and design of GFM converters have been extensively discussed in the last few years, the estimation of grid frequency, a key variable for the GFM operation, has not been properly addressed. As a consequence, the real control performance of GFM converters can be different from the expected control performance. The selection and tuning of frequency estimator are relevant for the manufacturers. There are still some open questions regarding the design of frequency estimator, and how to tune it or where to estimate the frequency. The lack of consideration of the effect of frequency estimator in the synchronization control has generated two main problems. On the one hand, the poor choice of a frequency estimator or control configuration can provoke an unstable system, which is undesirable. On the other hand, the lack of a proper definition of frequency estimator evokes an inaccurate provision of the desired services or GFM capabilities, due to the bad provision or coupling between inertia, damping, and frequency response.

Previous work in the literature has addressed the GFM control structures and the effect of frequency estimator. Reference [5] concludes that the virtual synchronous machine (VSM) and droop are equivalent when the frequency estimator is not implemented. In [6], it is claimed that the power reference tracking is more precise using a phase-locked loop (PLL) when implementing the droop, but there is no discussion on the selection and tuning of frequency estimator. In [7], it is highlighted that the design of GFM control plays a key role in the transient stability, but the impact of frequency estimators is not examined. Similarly, [8] examines the way that oscillations propagate in VSM-based systems due to the interaction between frequency and voltage but does not explore the influence of different frequency estimation methods on the oscillation behaviors. Reference [9] presents a detailed analysis of how frequency and voltage interactions

Manuscript received: February 19, 2025; revised: May 15, 2025; accepted: September 19, 2025. Date of CrossCheck: September 19, 2025. Date of online publication: November 12, 2025.

This work was supported by the European Union's Next Generation PRTR program (FAIR project), with reference TED2021-129796B-C22.

The work of Oriol Gomis-Bellmunt was supported by the Institució Catalana de Recerca i Estudis Avançats (ICREA) Academia Program.

This article is distributed under the terms of the Creative Commons Attribution 4.0 International License (<http://creativecommons.org/licenses/by/4.0/>).

J. Girona-Badia (corresponding author), J. C. Olives-Camps, V. A. Lacerda, E. Prieto-Araujo, and O. Gomis-Bellmunt are with CITCEA-UPC, Department of Electrical Engineering, Universitat Politècnica de Catalunya, Barcelona, Spain (e-mail: jaume.girona@upc.edu; juan.carlos.olives@upc.edu; vinicius.lacerda@upc.edu; eduardo.prietoaraujo@upc.edu; oriol.gomis@upc.edu).

DOI: 10.35833/MPCE.2025.000144



in GFM VSGs can lead to self-sustained or induced oscillations. References [10] and [11] address the transient stability in VSGs under current saturation and mode-switching control but do not consider the role of frequency estimators. In [12] and [13], the synchronization control strategies that estimate frequency based on power measurements are presented; however, they rely on a non-industry-class control architecture.

To the author's best knowledge, no study has yet investigated the effect of the frequency estimator in the GFM synchronization control. Also, it has not yet discussed the tuning and structure of frequency estimator for GFM control and its effect on the synchronization of GFM and grid. To this end, this paper presents a novel analysis regarding the behavior and stability of GFM synchronization control with the frequency estimator. Further, the structure, tuning, and AC voltage measurement point of frequency estimator are investigated. Aiming to address these challenges, this paper provides the following main contributions.

1) This paper evaluates the impact of frequency estimator in the GFM synchronization control and static frequency response.

2) Different configurations are analyzed, taking into account the following.

① The industry-class synchronization control implementations: the VSM and droop.

② The AC voltage measurement point employed by the frequency estimator.

③ The structure of frequency estimator: the PLL, frequency-locked loop (FLL), and a first-order filter of the converter frequency.

④ The tuning of frequency estimator.

3) This paper describes the system behavior under different configurations both analytically and numerically. Moreover, the stability is discussed.

## II. ANALYTICAL COMPARISON

The GFM controllers require a synchronization control to function correctly. There are two main industry-class synchronization control implementations: the VSM and droop. Both synchronization control structures employ the grid frequency as input, as shown in Fig. 1. In this section, an analytical comparison is conducted under different configurations considering two synchronization control implementations, different types of frequency estimators (ideal frequency estimator, rated frequency of grid, PLL, and FLL), and two AC voltage measurement points for frequency estimators (the point of connection (PoC) and the point where the converter sets the frequency and voltage (MP<sub>AC</sub>), as shown in Fig. 2).

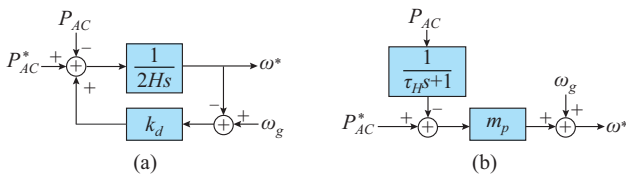


Fig. 1. Synchronization control structures. (a) VSM. (b) Droop.

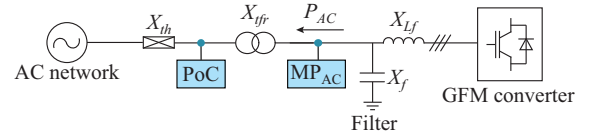


Fig. 2. GFM converter connected to AC network.

The analysis uses an equivalent formulation similar to the swing equation obtained from the control structure and AC grid equations. Moreover, a linearized model of the frequency estimators is employed. The equivalent formulation will permit the comparison of control functionalities (virtual inertia, damping, or frequency response) under different configurations. However, this analysis assumes that a proper AC voltage control is implemented [14] and the DC voltage is regulated.

The control functionalities analyzed in this paper, i.e., virtual inertia, damping, and static frequency response, are related to the control performance and can be defined as follows.

1) Virtual inertia: injection of energy due to a variation of frequency, which can be related to the energy provided by:

$$2H^* \Delta\omega \frac{S_b}{\omega_0} = E_H \quad (1)$$

where  $H^*$  is the global virtual inertia coefficient;  $S_b$  is the nominal power;  $\omega_0$  is the rated frequency;  $\Delta\omega$  is the variation of frequency; and  $E_H$  is the energy injected into AC network during the frequency variation. The virtual inertia is expressed in the equivalent formulation as  $2H\omega^*s$ , where  $\omega^*$  is the converter frequency; and  $H$  is the virtual inertia constant.

2) Damping: power that is injected to converge the converter frequency to the AC network frequency. The damping in the equivalent formulation is defined as  $k_d(\omega_g - \omega^*)$ , where  $k_d$  is the global damping coefficient; and  $\omega_g$  is the grid frequency.

3) Static frequency response: a static frequency support contribution, which provides power when there is a deviation of the converter frequency  $\omega^*$  with respect to the rated frequency  $\omega_0$ , expressed as  $\frac{1}{m_p}(\omega_0 - \omega^*)$  in the equivalent formulation, where  $\frac{1}{m_p}$  is the global static frequency response coefficient. This frequency support affects the power exchanged in the steady state.

### A. Ideal Frequency Estimator

In this subsection, a system behavior analysis will be carried out for both industry-class synchronization control implementations, considering an ideal frequency estimator, i.e., the frequency is obtained ideally from AC grid.

#### 1) VSM

The VSM is a synchronization control based on the synchronous machine characterized by the swing equation, and its structure is represented in Fig. 1(a). The VSM equation in the Laplace domain is expressed as:

$$\omega^* = \frac{1}{2Hs} [P_{AC}^* - P_{AC} + k_d(\omega_g - \omega^*)] \quad (2)$$

where  $P_{AC}^*$  is the reference power injected into AC network;

and  $P_{AC}$  is the actual power injected into AC network. Equation (2) can be reformulated as:

$$\underbrace{2H\omega^*s}_{\text{Virtual inertia}} = P_{AC}^* - P_{AC} + \underbrace{k_d(\omega_g - \omega^*)}_{\text{Damping}} \quad (3)$$

It can be seen that the virtual inertia is defined by  $2H$ . Also, it does not provide a static frequency response.

## 2) Droop

The droop is a synchronization control based on the behavior of governor turbine, and its structure is shown in Fig. 1(b). The droop equation in the Laplace domain is expressed as:

$$\omega^* = \omega_g + m_p \left( P_{AC}^* - \frac{1}{\tau_H s + 1} P_{AC} \right) \quad (4)$$

where  $m_p$  is the power-frequency droop constant; and  $\tau_H$  is the time constant of low-pass filter, which is expected to emulate the virtual inertia. Considering that  $P_{AC}^*$  is constant and its derivative is equal to zero, the equivalent formulation of droop with an ideal frequency estimator can be expressed as:

$$\frac{\tau_H}{m_p} s(\omega^* - \omega_g) = P_{AC}^* - P_{AC} + \underbrace{\frac{1}{m_p}(\omega_g - \omega^*)}_{\text{Damping}} \quad (5)$$

From (5), it can be seen that this configuration does not emulate the virtual inertia since there is no  $s\omega^*$  term in (5), which will be validated in Section IV. Nevertheless, it has the term  $s(\omega^* - \omega_g)$ , which does not match the effect of virtual inertia, as will be demonstrated in Section IV. Furthermore, the damping is emulated with a global damping coefficient equivalent to  $\frac{1}{m_p}$ .

In conclusion, if the frequency is obtained ideally from the AC grid, the behaviors of the VSM (3) and droop (5) are not equivalent. Moreover, the droop does not emulate the virtual inertia. Note that the system does not provide a static frequency response.

## B. Rated Frequency of Grid

In this subsection, the grid frequency  $\omega_g$  is set to its rated frequency ( $\omega_g = \omega_0$ ) to observe the effect of a constant value on the synchronization dynamics.

### 1) VSM

The equivalent formulation of VSM in the Laplace domain considering the rated frequency of grid is expressed as:

$$\underbrace{2H\omega^*s}_{\text{Virtual inertia}} = P_{AC}^* - P_{AC} + \underbrace{k_d(\omega_0 - \omega^*)}_{\text{Static frequency response}} \quad (6)$$

The virtual inertia coefficient is equivalent to  $2H$ . The system has no damping (since the term  $(\omega_g - \omega^*)$  does not appear) but has static frequency response.

### 2) Droop

From (5), considering  $\omega_0$  is constant and its derivative is equal to 0, the equivalent formulation of droop in the Laplace domain considering the rated frequency of grid is expressed as:

$$\underbrace{\frac{\tau_H}{m_p} \omega^* s}_{\text{Virtual inertia}} = P_{AC}^* - P_{AC} + \underbrace{\frac{1}{m_p}(\omega_0 - \omega^*)}_{\text{Static frequency response}} \quad (7)$$

Comparing the equivalent formulations of VSM (6) and droop (7), it can be deduced that they both emulate virtual inertia, provide a static frequency response, and do not consider the damping. Additionally, if  $\frac{\tau_H}{m_p} = 2H$ ,  $\frac{1}{m_p} = k_d$ , and  $\omega_g = \omega_0$ , they exhibit the same behaviors, as demonstrated in [5]. If a static frequency response is not desired,  $\omega_g$  cannot be set as a constant, and the grid frequency needs to be estimated.

## C. PLL

In this subsection, a synchronous reference frame phase-locked loop (SRF-PLL) tracks the grid frequency needed in the synchronization control. The system dynamics of PLL can be obtained by linearizing the closed loop considering small angle errors [15], [16]:

$$\frac{\hat{\theta}_g(s)}{\theta_g(s)} = \frac{2\zeta\omega_n s + \omega_n^2}{s^2 + 2\zeta\omega_n s + \omega_n^2} \quad (8)$$

where  $\hat{\theta}_g$  and  $\theta_g$  are the estimated and real angles of grid, respectively;  $\zeta$  is the damping; and  $\omega_n$  is the natural frequency. Equation (8) is also equivalent to:

$$\frac{\hat{\omega}_g(s)}{\omega_g(s)} = \frac{2\zeta\omega_n s + \omega_n^2}{s^2 + 2\zeta\omega_n s + \omega_n^2} \quad (9)$$

where  $\hat{\omega}_g$  is the estimated frequency of grid. The PLL implements a proportional-integral (PI) controller, whose transfer function is defined as [15], [16]:

$$K_{PLL}(s) = k_p \frac{\tau_{PLL} s + 1}{\tau_{PLL} s} \quad (10)$$

where  $\tau_{PLL}$  is the time constant of PLL; and  $k_p$  is the proportional gain of PI controller. To relate (9) and PI control parameters, the following parameters must be considered:

$$\begin{cases} \omega_n = \sqrt{\frac{k_p E_m}{\tau_{PLL}}} \\ \zeta = \frac{\sqrt{\tau_{PLL} k_p E_m}}{2} \end{cases} \quad (11)$$

where  $E_m$  is the peak AC voltage.

Here, two possible AC voltage measurement points, PoC and MP<sub>AC</sub>, for the PLL are considered. Note that in the MP<sub>AC</sub> case,  $\omega_g$  will be the same as  $\omega^*$  (considering that the voltage is properly controlled), since the AC voltage used is the same as the one when the converter sets frequency to  $\omega^*$ .

### 1) VSM with PLL at PoC

If the PLL is employed at the PoC utilizing the VSM (see Fig. 3(a)), its behavior can be obtained by applying (9) to (3), resulting in:

$$2H\omega^*s = P_{AC}^* - P_{AC} + k_d \left( \frac{2\zeta\omega_n s + \omega_n^2}{s^2 + 2\zeta\omega_n s + \omega_n^2} \omega_g - \omega^* \right) \quad (12)$$

Multiplying (12) by  $s^2 + 2\zeta\omega_n s + \omega_n^2$ , the synchronization control behavior can be defined as:

$$2H\omega^*s(s^2 + 2\zeta\omega_n s + \omega_n^2) = (P_{AC}^* - P_{AC})(s^2 + 2\zeta\omega_n s + \omega_n^2) + k_d[(2\zeta\omega_n s + \omega_n^2)\omega_g - (s^2 + 2\zeta\omega_n s + \omega_n^2)\omega^*] \quad (13)$$

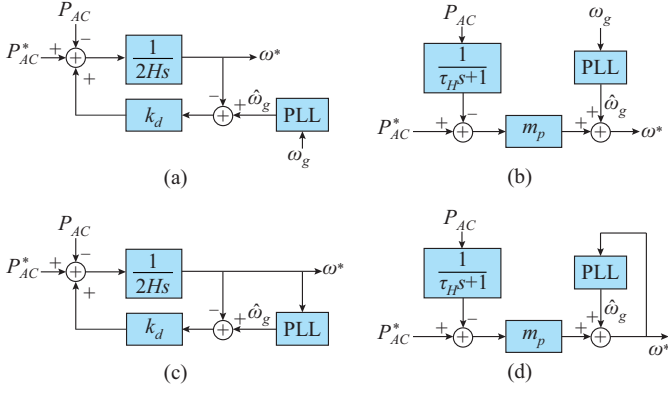


Fig. 3. Synchronization control schemes under different PLL configurations. (a) VSM with PLL at PoC. (b) Droop with PLL at PoC. (c) VSM with PLL at  $MP_{AC}$ . (d) Droop with PLL at  $MP_{AC}$ .

If the voltage is assumed constant, the AC network is inductive, and only small variations of phase are considered, the derivative of  $P_{AC}$  can be defined as [12], [17]:

$$P_{AC}s = \frac{U_{VSC}U_{AC}}{X_{AC}}(\omega^* - \omega_g) \quad (14)$$

where  $U_{VSC}$  is the modulated voltage by the converter;  $U_{AC}$  is the AC network voltage; and  $X_{AC}$  is the AC equivalent inductance, which may include the virtual admittance if added.

Substituting (14) into (13) yields:

$$\begin{aligned} \frac{2H}{\omega_n^2} \omega^* s^3 + \left( \frac{4H\zeta}{\omega_n} + \frac{k_d}{\omega_n^2} \right) \omega^* s^2 + \frac{2H\omega^* s}{\text{Virtual inertia}} + \\ \left( \frac{U_{VSC}U_{AC}}{X_{AC}\omega_n^2} + \frac{k_d 2\zeta}{\omega_n} \right) s(\omega^* - \omega_g) = \\ P_{AC}^* - P_{AC} + \underbrace{\left( \frac{2\zeta}{\omega_n} \frac{U_{VSC}U_{AC}}{X_{AC}} + k_d \right)}_{\text{Damping}} (\omega_g - \omega^*) \end{aligned} \quad (15)$$

From (15), the following conclusions for VSM with PLL at PoC are obtained.

- 1) The virtual inertia emulated is maintained at  $2H$ .
- 2) The damping is affected by the PLL dynamics and damping parameter.
- 3) It does not have static frequency response.
- 4) Several new parameters such as the terms  $s^2\omega^*$ ,  $s^3\omega^*$ , and  $s(\omega^* - \omega_g)$  appear, which are not corresponding to the virtual inertia, damping, or static frequency response.

#### 2) Droop with PLL at PoC

The equivalent formulation of the droop with PLL at the PoC can be defined as (using (5), (9) and (14)):

$$\begin{aligned} \left( \frac{2\zeta}{\omega_n} \frac{\tau_H}{m_p} s + \frac{\tau_H}{m_p} + \frac{2\zeta}{m_p \omega_n} + \frac{U_{VSC}U_{AC}}{X_{AC}\omega_n^2} \right) s(\omega^* - \omega_g) + \\ \frac{\tau_H}{m_p \omega_n^2} \omega^* s^3 + \frac{1}{m_p \omega_n^2} \omega^* s^2 = P_{AC}^* - P_{AC} + \\ \underbrace{\left( \frac{2\zeta}{\omega_n} \frac{U_{VSC}U_{AC}}{X_{AC}} + \frac{1}{m_p} \right)}_{\text{Damping}} (\omega_g - \omega^*) \end{aligned} \quad (16)$$

From (16), the following conclusions for droop with PLL at PoC are obtained.

- 1) It does not emulate the virtual inertia since the param-

eter  $s\omega^*$  does not appear.

- 2) The damping is influenced by the PLL tuning and  $1/m_p$ .
- 3) It does not have a static frequency response.
- 4) Several additional parameters such as the terms  $s(\omega^* - \omega_g)$ ,  $s^3\omega^*$ , and  $s^2\omega^*$  appear, which are not desired and affect the frequency response.

#### 3) VSM with PLL at $MP_{AC}$

When the AC voltage measurement point changes to  $MP_{AC}$  for VSM with PLL, as shown in Fig. 3(c), the synchronization control behavior can be defined as:

$$2H\omega^* s = P_{AC}^* - P_{AC} + k_d \omega^* \left( \frac{2\zeta \omega_n s + \omega_n^2}{s^2 + 2\zeta \omega_n s + \omega_n^2} - 1 \right) \quad (17)$$

Substituting (14) into (17), the equivalent formulation can be defined as:

$$\begin{aligned} \frac{2H}{\omega_n^2} \omega^* s^3 + \left( \frac{4H\zeta}{\omega_n} + \frac{k_d}{\omega_n^2} \right) \omega^* s^2 + \frac{2H\omega^* s}{\text{Virtual inertia}} + \frac{U_{VSC}U_{AC}}{X_{AC}\omega_n^2} s(\omega^* - \omega_g) = \\ P_{AC}^* - P_{AC} + \underbrace{\frac{2\zeta}{\omega_n} \frac{U_{VSC}U_{AC}}{X_{AC}}}_{\text{Damping}} (\omega_g - \omega^*) \end{aligned} \quad (18)$$

The effect of the AC voltage measurement point for PLL on the equivalent formulation and synchronization control behavior can be observed by comparing (18) and (15). If the AC voltage measurement point is located at  $MP_{AC}$ , the following terms are omitted in Laplace domain:

- 1)  $\frac{2k_d \zeta}{\omega_n} s(\omega^* - \omega_g)$ .
- 2)  $k_d(\omega_g - \omega^*)$ . The damping does not depend on  $k_d$  and is reduced. And it only depends on the PLL tuning and grid characteristics.

#### 4) Droop with PLL at $MP_{AC}$

The following case study is the droop that employs a PLL at the  $MP_{AC}$ . Its equivalent formulation can be defined as (using Fig. 3(d) and (14)):

$$\begin{aligned} \frac{U_{VSC}U_{AC}}{X_{AC}\omega_n^2} s(\omega^* - \omega_g) + \frac{\tau_H}{m_p \omega_n^2} \omega^* s^3 + \frac{1}{m_p \omega_n^2} \omega^* s^2 = \\ P_{AC}^* - P_{AC} + \underbrace{\frac{2\zeta}{\omega_n} \frac{U_{VSC}U_{AC}}{X_{AC}}}_{\text{Damping}} (\omega_g - \omega^*) \end{aligned} \quad (19)$$

If the PLL measurement point is placed at the  $MP_{AC}$  (19) instead of PoC (16), the following terms disappear:

- 1)  $\left( \frac{2\zeta}{\omega_n} \frac{\tau_H}{m_p} s + \frac{\tau_H}{m_p} + \frac{2\zeta}{m_p \omega_n} \right) s(\omega^* - \omega_g)$ .
- 2)  $\frac{1}{m_p} (\omega^* - \omega_g)$ . The damping does not depend on  $m_p$  and is reduced.

Locating the PLL at the PoC increases the damping and stability in the droop and VSM. This is further demonstrated in Sections III-B and VI.

#### D. FLL

The FLL implemented in this paper is the second-order generalized integrator frequency-locked loop (SOGI-FLL), as shown in Fig. 4, which has two parameters to tune:  $\gamma$  (integral controller gain) and  $k$  (bandwidth of band-pass filter). In [18], it is explained that if  $k = \sqrt{2}$ , the SOGI-FLL dynamics

are expressed as:

$$\frac{\hat{\omega}_g(s)}{\omega_g(s)} = \frac{1}{\tau_{f,\omega}s + 1} \quad (20)$$

where  $\tau_{f,\omega} = 1/\gamma$ .

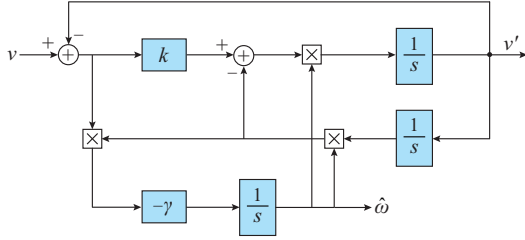


Fig. 4. Structure of FLL-SOGI.

In this subsection, the FLL is applied to the VSM and droop at the PoC and  $MP_{AC}$ . As explained in Section II-C, when the AC voltage measurement point for FLL is placed at the  $MP_{AC}$ ,  $\omega_g$  is equal to  $\omega^*$ , as shown in Fig. 5. In [19]-[22], the structure shown in Fig. 5(c) is used as a synchronization control, employing a filter to estimate the grid frequency. The same structure can also represent the VSM with an FLL that measures the frequency at  $MP_{AC}$ . Moreover, this structure is also equivalent to implementing a low-pass filter in the VSM case since:

$$\frac{1}{\tau_{f,\omega}s + 1} \omega^* - \omega^* = -\frac{\tau_{f,\omega}s}{\tau_{f,\omega}s + 1} \omega^* \quad (21)$$

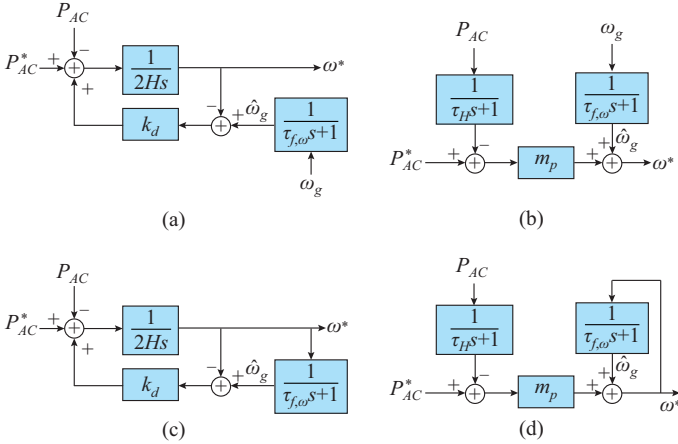


Fig. 5. Synchronization control schemes under different FLL configurations. (a) VSM with FLL at PoC. (b) Droop with FLL at PoC. (c) VSM with FLL at  $MP_{AC}$  or with a low-pass filter to define grid frequency. (d) Droop with FLL at  $MP_{AC}$ .

### 1) VSM with FLL at PoC

The effect of implementing a VSM with FLL at the PoC is analyzed below. The equivalent formulation can be obtained from Fig. 5(a) and (14):

$$2\tau_{f,\omega}H\omega^*s^2 + \underbrace{(2H + k_d\tau_{f,\omega})\omega^*s}_{\text{Virtual inertia}} = P_{AC}^* - P_{AC} + \underbrace{\left(\frac{U_{VSC}U_{AC}}{X_{AC}}\tau_{f,\omega} + k_d\right)(\omega_g - \omega^*)}_{\text{Damping}} \quad (22)$$

By comparing (15) and (22), different dynamics of FLL

and PLL lead to differences depending on the frequency estimator employed. The relevant conclusions from (22) are:

1) The global virtual inertia coefficient is  $2H + k_d\tau_{f,\omega}$ , which means that the virtual inertia emulated also depends on the FLL tuning and  $k_d$ .

2) The damping depends on  $\frac{U_{VSC}U_{AC}}{X_{AC}}\tau_{f,\omega}$  and  $k_d$ .

3) The additional parameter  $s^2\omega^*$  appears.

### 2) Droop with FLL at PoC

The equivalent formulation of the droop with an FLL at the PoC can be obtained from Fig. 5(b) and (14):

$$\frac{\tau_H\tau_{f,\omega}}{m_p}\omega^*s^2 + \underbrace{\frac{\tau_{f,\omega}}{m_p}\omega^*s}_{\text{Virtual inertia}} = P_{AC}^* - P_{AC} + \underbrace{\left(\frac{U_{VSC}U_{AC}}{X_{AC}}\tau_{f,\omega} + \frac{1}{m_p}\right)(\omega_g - \omega^*)}_{\text{Damping}} \quad (23)$$

As in the VSM, using FLL increases the virtual inertia emulated, as shown in (16) and (23). The main characteristics of this configuration are:

1)  $\frac{\tau_{f,\omega}}{m_p}$  defines the virtual inertia emulated, which does not depend on  $\tau_H$  and is influenced by the FLL tuning and  $m_p$ .

2) The damping of system is defined by  $\frac{U_{VSC}U_{AC}}{X_{AC}}\tau_{f,\omega} + \frac{1}{m_p}$ .

3) There are additional parameters, i.e.,  $s^2\omega^*$  and  $s(\omega_g - \omega^*)$ .

### 3) VSM with FLL at $MP_{AC}$

The equivalent formulation of VSM with an FLL at the  $MP_{AC}$  can be obtained from Fig. 5(c) and (14):

$$2\tau_{f,\omega}H\omega^*s^2 + \underbrace{(2H + k_d\tau_{f,\omega})\omega^*s}_{\text{Virtual inertia}} = P_{AC}^* - P_{AC} + \underbrace{\frac{U_{VSC}U_{AC}}{X_{AC}}\tau_{f,\omega}(\omega_g - \omega^*)}_{\text{Damping}} \quad (24)$$

The main difference at different measurement points for FLL using the VSM is the damping. When comparing (22) and (24), it can be observed that the parameter  $k_d$  disappears from the damping when the FLL is connected to  $MP_{AC}$ , reducing the damping and the capability to tune it.

### 4) Droop with FLL at $MP_{AC}$

The equivalent formulation of droop with an FLL at the  $MP_{AC}$  can be obtained from Fig. 5(d) and (14):

$$\frac{\tau_H\tau_{f,\omega}}{m_p}\omega^*s^2 + \underbrace{\frac{\tau_{f,\omega}}{m_p}\omega^*s}_{\text{Virtual inertia}} = P_{AC}^* - P_{AC} + \underbrace{\frac{U_{VSC}U_{AC}}{X_{AC}}\tau_{f,\omega}(\omega_g - \omega^*)}_{\text{Damping}} \quad (25)$$

When the measurement point for FLL is placed at the  $MP_{AC}$ , the two following parameters disappear:

1)  $\frac{1}{m_p}(\omega_g - \omega^*)$ . This leads to a damping that only depends on  $\frac{U_{VSC}U_{AC}}{X_{AC}}\tau_{f,\omega}$ , and is not affected by  $m_p$ .

2)  $s(\omega_g - \omega^*)$ .

In Table I, there is a summary of the analytical analysis.

The most relevant point is that the addition of a frequency estimator leads to a system that does not provide static fre-

quency response. However, there are various problems related to the virtual inertia emulated and system behavior.

TABLE I  
SUMMARY OF ANALYTICAL ANALYSIS

Configuration	Synchronization control implementation	Virtual inertia ( $\omega^* s$ )	Damping ( $\omega_g - \omega^*$ )	Static frequency response	$s^{n+1} \omega^*$ ( $n \in \mathbb{N}$ )	$s^n (\omega_g - \omega^*)$ ( $n \in \mathbb{N}$ )
Rated frequency of grid ( $\omega_0$ )	VSM	✓	×	✓	×	×
	Droop	✓	×	✓	×	×
PLL at PoC	VSM	✓	✓	×	✓	✓
	Droop	×	✓	×	✓	✓
PLL at MP <sub>AC</sub>	VSM	✓	✓ <sup>***</sup>	×	✓	✓
	Droop	×	✓ <sup>***</sup>	×	✓	✓
FLL at PoC	VSM	✓ <sup>*</sup>	✓	×	✓	×
	Droop	✓ <sup>**</sup>	✓	×	✓	✓
FLL at MP <sub>AC</sub>	VSM	✓ <sup>*</sup>	✓ <sup>***</sup>	×	✓	×
	Droop	✓ <sup>**</sup>	✓ <sup>***</sup>	×	✓	×

Note: the symbols ✓ and × represent that the corresponding term appears and does not appear, respectively; the superscript \* represents that the virtual inertia emulated does not depend only on  $H$  or  $\tau_H/m_p$ ; the superscript \*\* represents that the virtual inertia emulated does not depend on  $H$  or  $\tau_H/m_p$ ; and the superscript \*\*\* represents that the damping coefficient is not affected by  $k_d$  or  $m_p$ .

There are relevant differences between the two industry-class synchronization control implementations. In the droop case, the parameter  $\tau_H/m_p$  does not define the system virtual inertia emulated. This discrepancy increases the difficulty of tuning the virtual inertia emulated or even renders the system incapable of emulating any virtual inertia. Nevertheless, the parameter  $H$  in the VSM always influences the virtual inertia emulated. Moreover, from Table I, it can be observed that employing the FLL results in an increase in the virtual inertia emulated. However, the PLL has a minor impact on the relevant functionalities. Additionally, the inclusion of a frequency estimator introduces side-effect dynamics into the synchronization control. Finally, the AC voltage measurement point for PLL or FLL affects the system damping, resulting in greater damping at the PoC.

### III. SYSTEM STABILITY

This section analyzes the stability under different configurations, taking into account various frequency estimator tunings. A simplified model of GFM converter connected to the AC network in Fig. 2 is utilized, as shown in Fig. 6. The voltage control and the fast dynamics of AC network are simplified to focus on the synchronization control.

#### A. Modeling

The modeling used in this subsection is explained in [17]. As shown in Fig. 6, the simplified model has three parts: the power exchange, AC network synchronization control, and converter synchronization control.

The GFM converter is modeled as a controlled voltage source, whose voltage magnitude is constant and voltage phase is set by the power synchronization control, which depends on the configuration selected. To represent the frequency estimators, (9) and (20) are utilized.

The AC network is modeled as an ideal voltage source with the mechanical dynamics of a non-reheat steam turbine

from [23], and it is assumed to have an ideal voltage regulation.

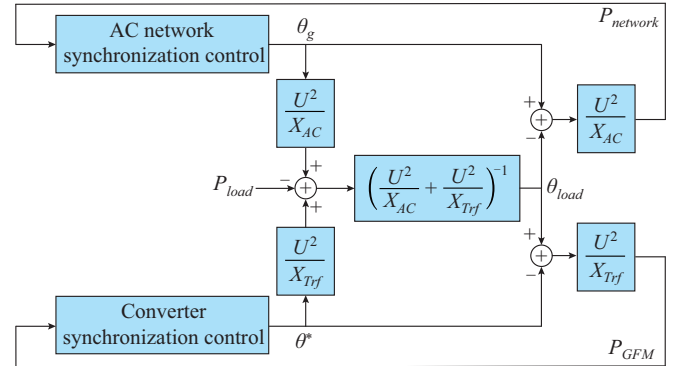


Fig. 6. Simplified system of GFM converter connected to AC network.

To represent the power exchange between the converter and AC network, the following assumptions are made:

- 1) The voltage is considered constant.
- 2) The network dynamics are omitted for this analysis to focus the study on the inertial-related dynamics.
- 3) The variation of phase is small ( $\sin(\theta_1 - \theta_2) \approx \theta_1 - \theta_2$ ).

Using these assumptions, the power flow of an inductive line can be calculated as:

$$P = \frac{U_1 U_2}{X_{1-2}} (\theta_1 - \theta_2) \quad (26)$$

where  $U_1$  and  $U_2$  are the voltage amplitudes at both ends of the line;  $X_{1-2}$  is the line inductance; and  $\theta_1$  and  $\theta_2$  are the voltage phases at both ends of the line [12], [17].

If the load is connected at the PoC of AC network and GFM converter, its power  $P_{load}$  is expressed as:

$$P_{load} = P_{network} + P_{GFM} \quad (27)$$

where  $P_{network}$  and  $P_{GFM}$  are the power of AC network and GFM converter, respectively.

Equations (26) and (27) enable the representation of a lin-

earized system of power interactions, as shown Fig. 6.

### B. Pole Analysis

In this subsection, the system poles are analyzed using the

mentioned modeling under different configurations and several frequency estimator tunings, as shown in Figs. 7-10. Supplementary Material A presents the validation of the modeling method.

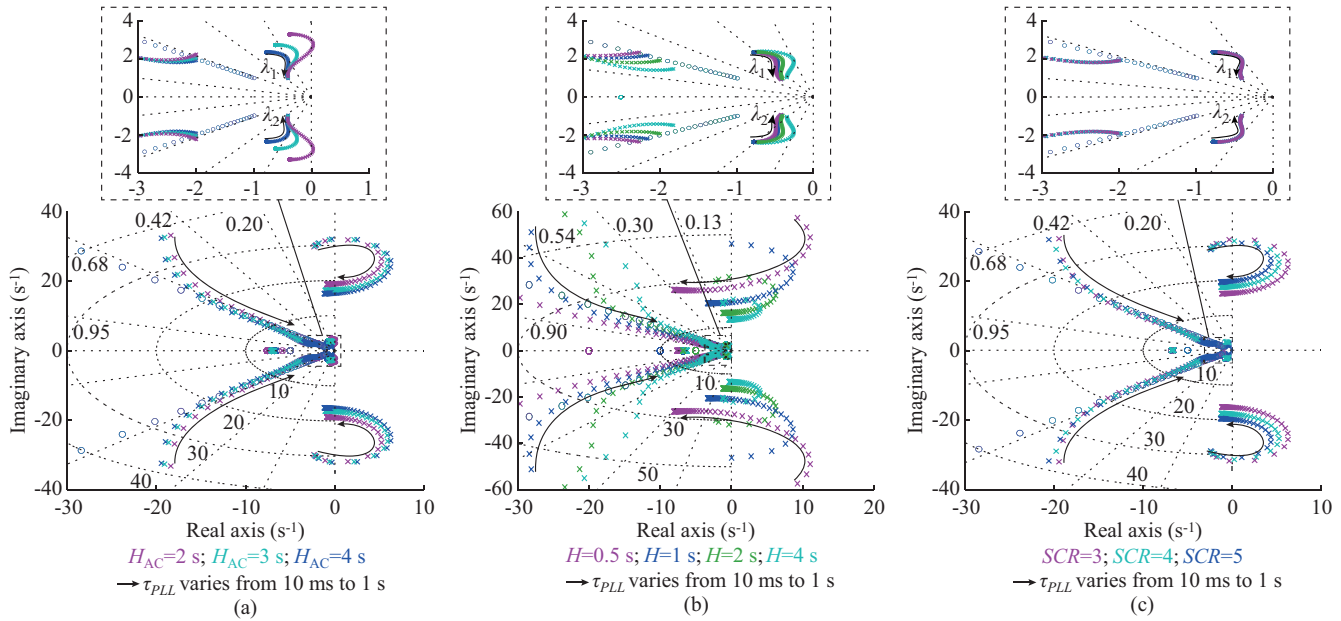


Fig. 7. Pole trajectories with varying  $\tau_{PLL}$  from 10 ms to 1 s for droop with PLL at PoC with a sensitivity analysis of AC network inertia, virtual inertia, and SCR. (a) AC network inertia. (b) Virtual inertia. (c) SCR.

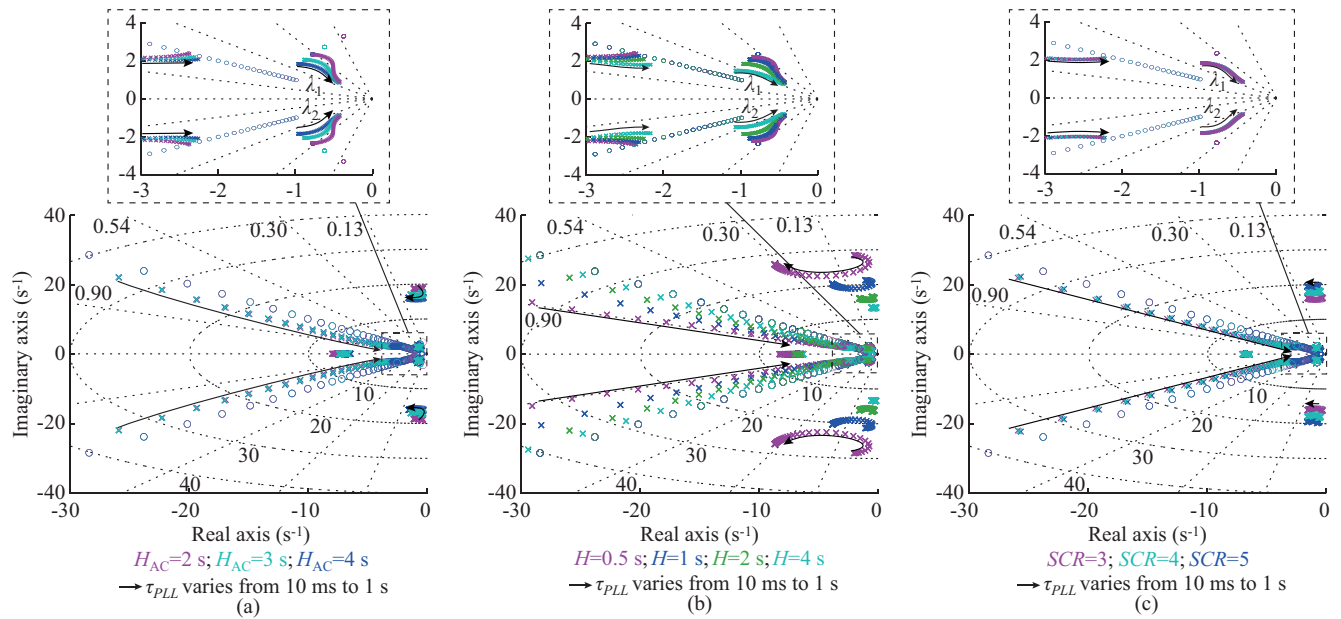


Fig. 8. Pole trajectories with varying  $\tau_{PLL}$  from 10 ms to 1 s for VSM with PLL at PoC with a sensitivity analysis of AC network inertia, virtual inertia, and SCR. (a) AC network inertia. (b) Virtual inertia. (c) SCR.

In Figs. 7-10, when the frequency estimator is at the PoC, different AC network inertia (represented by  $H_{AC}$ ), virtual inertia (represented by  $H$ ), and short circuit ratios (SCRs) are considered for the sensitivity analysis. Figures 11-13 show the pole trajectories at the  $MP_{AC}$  (in green) and POC (in blue) for PLL and FLL.

The main difference between the two industry-class synchronization control implementations, when the frequency es-

timator uses the AC voltage from the PoC, is that the VSM is stable for all the analyzed scenarios. Nevertheless, the droop has several unstable cases depending on the frequency estimator tuning. The system is stable for fast PLLs ( $\tau_{PLL} \leq 30$  ms), slow PLL ( $\tau_{PLL} \geq 500$  ms), and FLL ( $\tau_{f,\omega} \geq 500$  ms).

The AC network inertia affects all configurations equally, and the damping is reduced with the reduction of the AC network inertia. Moreover, it can lead to instabilities such as for the droop with PLL, as shown in Fig. 7(a). Regarding

the virtual inertia emulated by the converters, the smaller the virtual inertia, the smaller the damping. If the SCR decreases, it produces an increase in the damping with the exception of droop with a fast PLL, which implies that the GFM

operates better with low SCR. The increase in the response time of frequency estimator raises the system damping and moves the system poles to the left, except in the case of droop with PLL, where the poles  $\lambda_1$  and  $\lambda_2$  are slower.

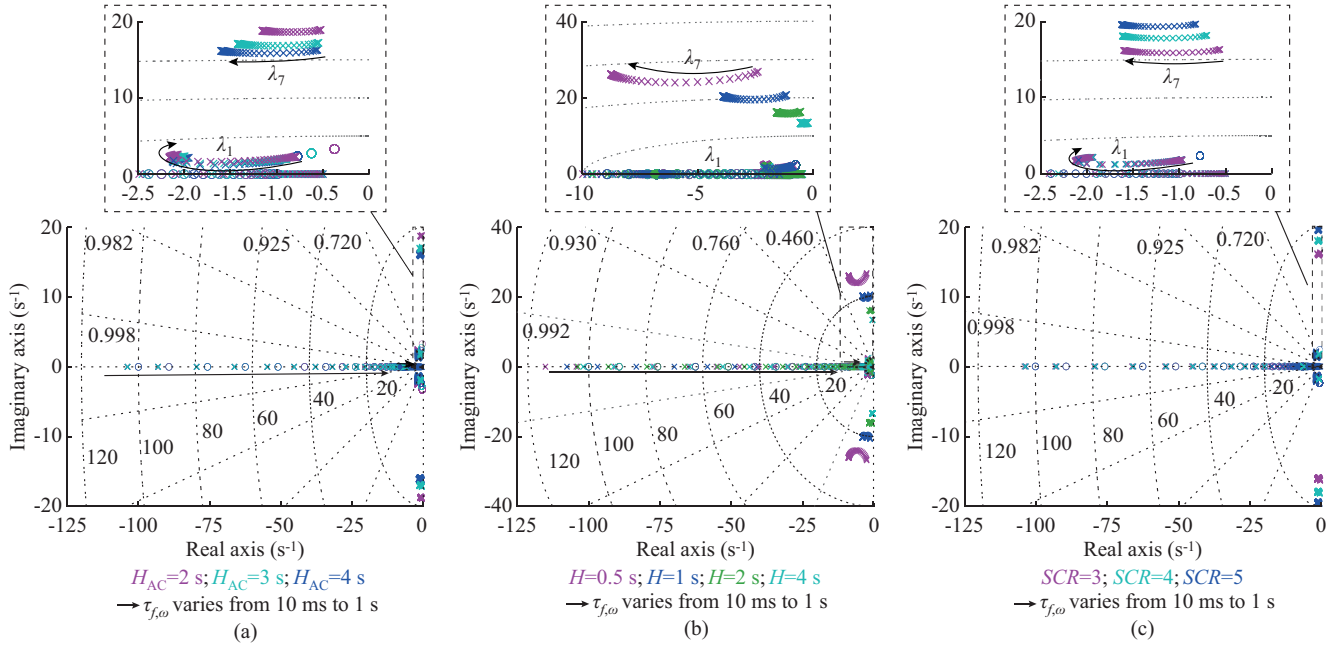


Fig. 9. Pole trajectories with varying  $\tau_{f,\omega}$  from 10 ms to 1 s for VSM with FLL at PoC with a sensitivity analysis of AC network inertia, virtual inertia, and SCR. (a) AC network inertia. (b) Virtual inertia. (c) SCR.

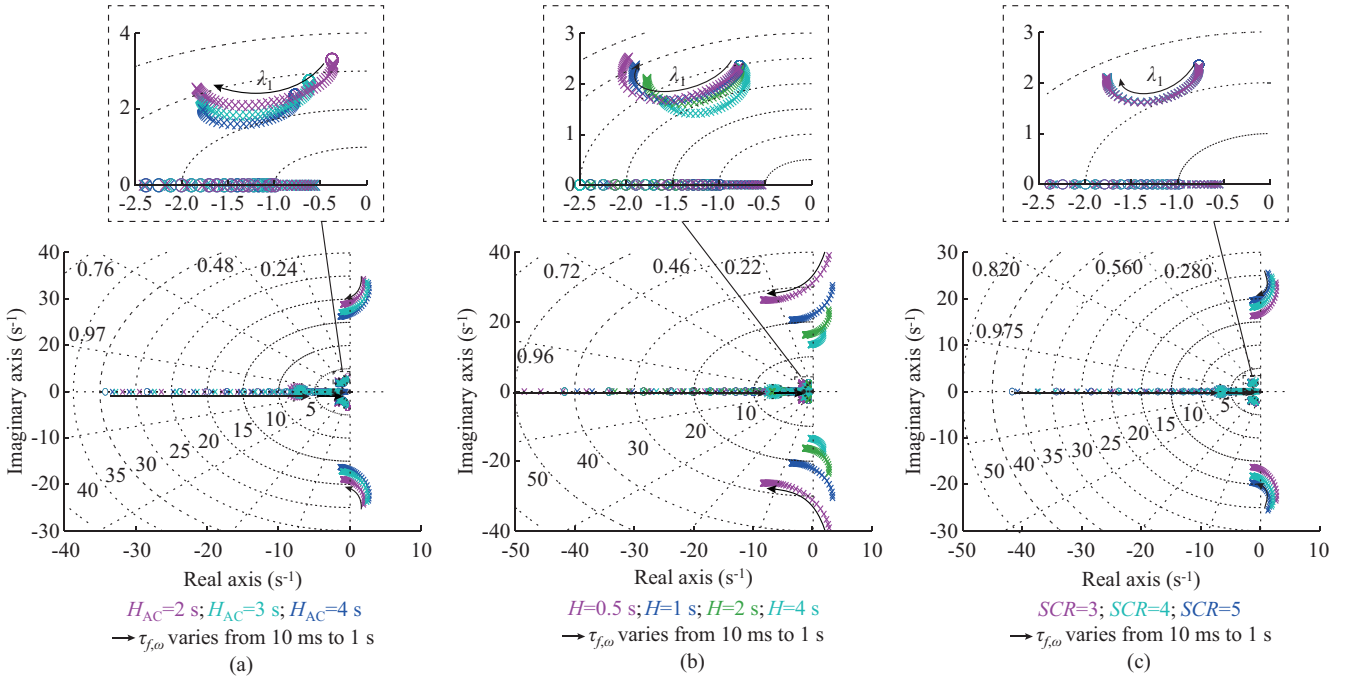


Fig. 10. Pole trajectories with varying  $\tau_{f,\omega}$  from 10 ms to 1 s for droop with FLL at PoC with a sensitivity analysis of AC network inertia, virtual inertia, and SCR. (a) AC network inertia. (b) Virtual inertia. (c) SCR.

As can be observed from Figs. 11-13, if the frequency estimator is placed at the  $MP_{AC}$  and but not at the PoC, the poles  $\lambda_7$  and  $\lambda_8$  are moved to the right, reducing the damping or making the system unstable in certain cases.

#### IV. DYNAMIC SIMULATIONS

In this section, the analytical and small-signal analyses are validated through time-domain simulations, which consider the full GFM control (voltage and synchronization control) and the dynamics related to the electrical grid. The param-

ters employed in these simulations are set in Supplementary Material B. The software employed is MATLAB Simulink.

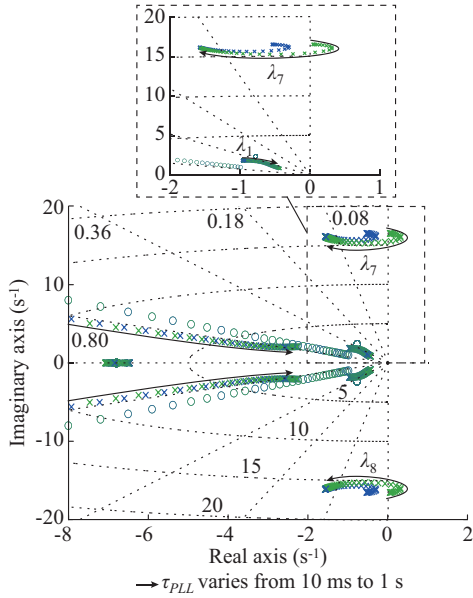


Fig. 11. Pole trajectories with varying  $\tau_{PLL}$  from 10 ms to 1 s for VSM with PLL at  $MP_{AC}$  and PoC.

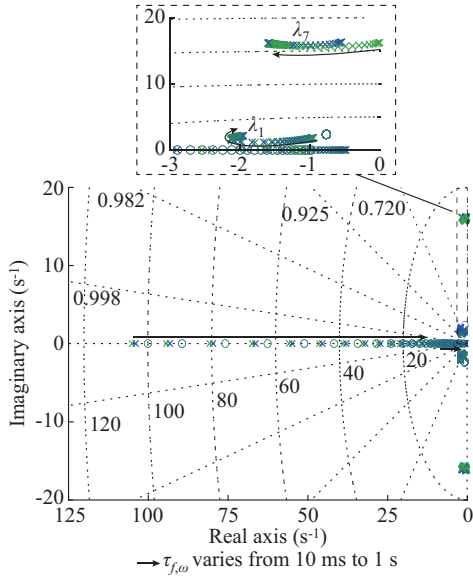


Fig. 12. Pole trajectories with varying  $\tau_{f,\omega}$  from 10 ms to 1 s for VSM with FLL at  $MP_{AC}$  and at PoC.

In Fig. 14, the dynamic simulation of a load connection under different analyzed configurations is shown, considering three different response time (10 ms, 100 ms, and 500 ms) of frequency estimator. The integral of the AC power, which represents the energy injected into the AC grid, will allow the exploration of the emulated virtual inertia if the system does not have a static frequency response. The different configurations are only plotted if they are stable. The test performed is a load connection to the PoC.

Figure 14(a)-(c) depicts the cases with a time constant of frequency estimator equivalent to 10 ms. Additionally, it considers the configurations that employ the rated frequency of

the grid and a grid-following (GFL) control (with a PLL having  $\tau_{PLL} = 10$  ms). The GFL is implemented with both zero active and reactive power injections. Here, it can be seen that the stable configurations are the VSM with PLL, VSM with FLL, and droop with PLL at the PoC. It can be seen from Fig. 14 that if  $\omega_g = \omega_0$ , the system has frequency response (the power after the transient is not zero, and the energy increases with a ramp). When the time constant of frequency estimator is 10 ms, three groups of different responses appear:

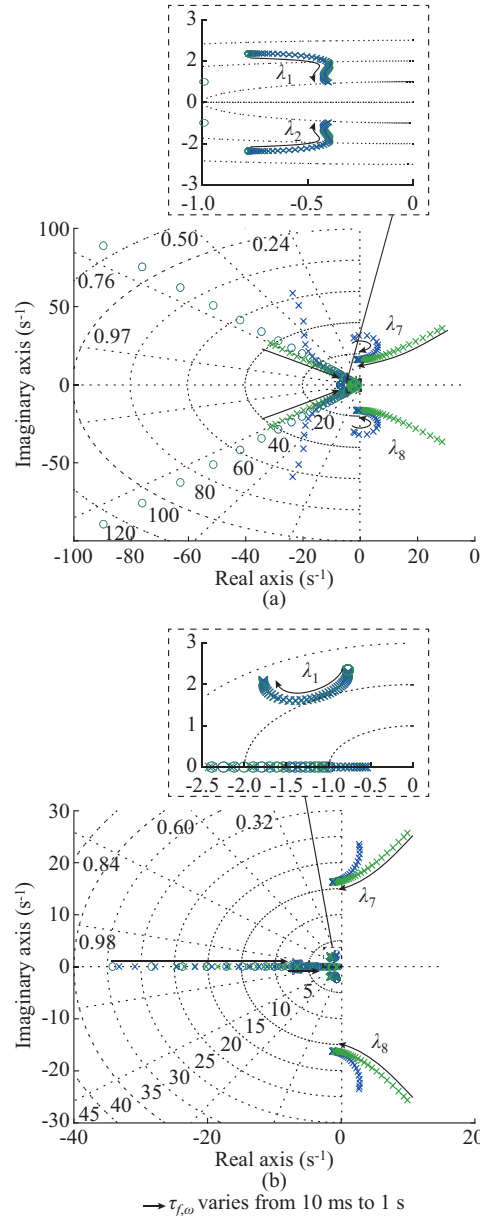


Fig. 13. Pole trajectories with varying  $\tau_{f,\omega}$  from 10 ms to 1 s for droop at  $MP_{AC}$  and PoC. (a) PLL. (b) FLL.

- 1) The droop and VSM when  $\omega_g = \omega_0$  are identical, as explained in [5].
- 2) The behaviors of the GFL and droop with a fast PLL are not identical in power. However, the frequency is equivalent and the emulated virtual inertia is 0 s in both cases, as demonstrated in Section II-C-2).

3) The VSMs with FLL and PLL have similar responses. Nevertheless, as anticipated in the analytical analysis (Section II-D-1), the virtual inertia coefficient is bigger (2.2 s)

in the FLL case. This is because the virtual inertia coefficient of the VSM with an FLL at the PoC is  $2H+k_d\tau_{f,\omega}$  as demonstrated in (22).

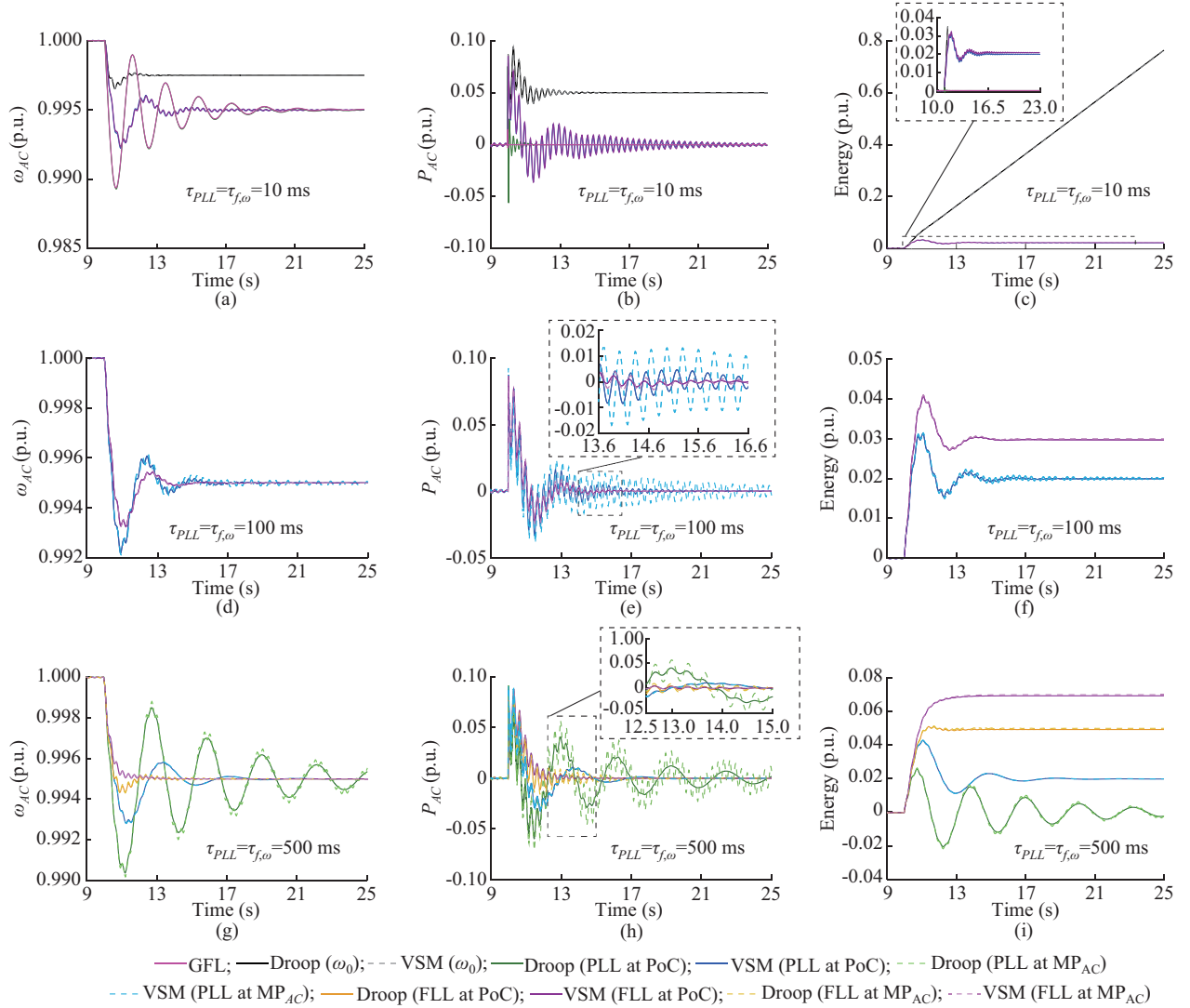


Fig. 14. Dynamic simulation of a load connection under different analyzed configurations. (a) Frequency when time constant of frequency estimator is 10 ms. (b) AC network power when time constant of frequency estimator is 10 ms. (c) Energy injected into AC grid when time constant of frequency estimator is 10 ms. (d) Frequency when time constant of frequency estimator is 100 ms. (e) AC network power when time constant of frequency estimator is 100 ms. (f) Energy injected into AC grid when time constant of frequency estimator is 100 ms. (g) Frequency when time constant of frequency estimator is 500 ms. (h) AC network power when time constant of frequency estimator is 500 ms. (i) Energy injected into AC grid when time constant of frequency estimator is 500 ms.

In conclusion, implementing a fast-tuned PLL in droop causes the system to behave similarly to a GFL. As a result, it fails to ensure the adequate frequency response capabilities of GFM. However, when a VSM is employed, there is a fast power injection immediately after the event, as required in GFM with inertia. Therefore, the employment of a frequency estimator does not necessarily endanger the GFM operation.

When the time constant of frequency estimator is 100 ms, the stable configurations are: the VSMs with FLL and PLL at PoC and  $MP_{AC}$ . As demonstrated in Section III-B, if  $\tau_{PLL}$  or  $\tau_{f,\omega}$  is equal to 100 ms, none of the droop cases are stable. There are two tendencies based on the frequency estimators used.

1) PLL: the virtual inertia coefficient is the expected one, i.e.,  $2H=4$  s.

2) FLL: the virtual inertia coefficient is not  $2H$ , and it is  $2H+k_d\tau_{f,\omega}=4+2=6$  s, as demonstrated in Sections II-D-1) and II-D-3).

The frequency estimator position affects the damping of system, as can be seen in the AC power in Fig. 14(e). If the PLL or FLL uses the PoC voltage, the system has fewer oscillations. This reduction of oscillations is equivalent to an increase in the damping. This tendency is consistent with Sections II-D-1) and II-D-3).

If the time constant of frequency estimator is 500 ms, all the analyzed cases are stable. The location of PLL or FLL mainly affects the damping of system, as shown in Table I

and Fig. 14(h). Also, the use of different frequency estimators affects the emulated virtual inertia to different degrees depending on the configuration, as shown in Fig. 14(i).

1) VSM with PLL: the virtual inertia coefficient is  $2H=4$  s.

2) VSM with FLL: the virtual inertia coefficient is  $2H+k_d\tau_{f,\omega}=4+10=14$  s, corresponding to an energy of 0.07 p.u. (using (1)), as demonstrated in Section II-C-3) and II-D-1).

3) Droop with PLL: the system has zero virtual inertia, and the energy provided after the event is equal to zero. This lack of virtual inertia is also represented in (16) and (19).

4) Droop with FLL: since the energy provided is 0.05 p.u., the virtual inertia coefficient is 10 s. As indicated in (23) and (25), the virtual inertia by the system depends on the tuning of FLL.

The dynamic simulations validate the analytical study (Section II) and stability analysis (Section III). These dynamic simulations also demonstrate that the frequency estimator and voltage control interactions do not affect the previously conducted studies.

## V. DISCUSSION

This section offers a discussion of the results derived from the previous analysis and assesses the most suitable configuration for the GFM synchronization control considering the GFM synchronization control structure as well as the structure, tuning, and AC voltage measurement point of frequency estimator.

### A. GFM Synchronization Control Structure

The different analyses show that the control structure affects the emulated virtual inertia: when the PLL is employed, the VSM emulates the expected virtual inertia and the droop emulates zero virtual inertia. However, when the FLL is utilized, the emulated virtual inertia increases in both cases.

The stability analysis in Section III-B shows that the system with droop is not stable under most configurations of frequency estimator. However, the system with VSM is stable under most configurations. The droop must be avoided when a frequency estimator is employed, due to its lack of controllability over emulated virtual inertia and its stability sensitivity to frequency estimator tuning. Even though VSM requires slightly more computing power, it remains the best-analyzed structure because it is inherently stable and less sensitive to the choice and tuning of frequency estimators. Moreover, it can emulate the designed virtual inertia when the PLL is employed.

### B. Structure of Frequency Estimator

The static frequency response is canceled when a frequency estimator is utilized. Moreover, as demonstrated in the analytical study and dynamic simulations, the structure and tuning of frequency estimator can impact the virtual inertia emulated by the converter. The PLL does not increase the emulated virtual inertia, which is desired since the virtual inertia is typically designed to be a constant parameter. However,

the FLL increases the emulated virtual inertia. The slower the FLL follows the frequency, the more virtual inertia is emulated, as shown in Fig. 14. Therefore, the PLL is more suitable as a frequency estimator, as it does not add additional virtual inertia regardless of its tuning.

### C. Tuning of Frequency Estimator

The frequency estimator adds dynamics not related to the primary goals such as virtual inertia, damping, or frequency response. The slower the frequency estimator is, the more significant the undesired dynamics are. The stability when the droop is employed is highly dependent on the tuning of frequency estimator. In contrast, the VSM is stable in all cases when the frequency estimator is connected to the PoC. When using the droop, the frequency estimator should be tuned carefully.

The best tuning of frequency estimator is the fastest one (around 10 ms), which could reduce the side-effect dynamics considering that the VSM is recommended (Section V-A). Especially when operating with an FLL, the tuning must be fast to avoid the addition of virtual inertia.

### D. AC Voltage Measurement Point of Frequency Estimator

The PoC is the most robust AC voltage measurement point for PLL or FLL. The system damping decreases when the frequency estimator is moved from the PoC to  $MP_{AC}$ . This also affects the stability of system. The frequency estimator has to be slower if the measurement is taken from  $MP_{AC}$  in order to keep the system stable.

## VI. CONCLUSION

This paper investigates the control performance of GFM synchronization control when a static frequency response is not desired. For this purpose, different GFM synchronization control structures and frequency estimator configurations have been evaluated. Three frequency estimators (the PLL, FLL, and a low-pass filter) implemented under two synchronization control implementations (the droop and VSM) are explored. Moreover, the AC voltage measurement point for the FLL or PLL and the tuning of frequency estimator are considered. To determine the optimal configuration, the analytical and stability studies are carried out, which are validated with time-domain simulations.

The results demonstrate that the frequency estimator effectively decouples the static frequency response from the synchronization control. Furthermore, the damping coefficient can be tuned as required. The absence of a static frequency response enables tracking the dispatched power. This configuration also allows the static frequency response to be added if necessary.

In conclusion, the best configuration is the VSM with a PLL at the PoC with fast tuning owing to its robustness, stability, control performance, and capability to provide a more stable response. Additionally, due to its inability to emulate inertia, the droop is not recommended to be implemented with a frequency estimator.

These recommendations will simplify the tuning and design of the GFM synchronization control, leading to im-

proved E-STATCOM, HVDC and IBR integration, and network stability.

## REFERENCES

- [1] European Council, "Directive 2009/28/EC of the European Parliament and of the Council of 23 April 2009 on the promotion of the use of energy from renewable sources," Brussels, Belgium, Tech. Rep., 2009.
- [2] D. Pattabiraman, R. H. Lasseter, and T. M. Jahns, "Comparison of grid following and grid forming control for a high inverter penetration power system," in *Proceedings of 2018 IEEE PES General Meeting*, Portland, USA, Aug. 2018, pp. 1-5.
- [3] F. Zhao, X. Wang, Z. Zhou *et al.*, "Comparative study of battery-based STATCOM in grid-following and grid-forming modes for stabilization of offshore wind power plant," *Electric Power Systems Research*, vol. 212, p. 108449, Nov. 2022.
- [4] B. Kroposki, B. Johnson, Y. Zhang *et al.*, "Achieving a 100% renewable grid: operating electric power systems with extremely high levels of variable renewable energy," *IEEE Power and Energy Magazine*, vol. 15, no. 2, pp. 61-73, Mar. 2017.
- [5] S. D'Arco and J. A. Suul, "Equivalence of virtual synchronous machines and frequency-droops for converter-based microgrids," *IEEE Transactions on Smart Grid*, vol. 5, no. 1, pp. 394-395, Jan. 2014.
- [6] E. Rokrok, T. Qoria, A. Bruyere *et al.*, "Effect of using PLL-based grid-forming control on active power dynamics under various SCR," in *Proceedings of 45th Annual Conference of the IEEE Industrial Electronics Society*, Lisbon, Portugal, Oct. 2019, pp. 4799-4804.
- [7] D. Pan, X. Wang, F. Liu *et al.*, "Transient stability of voltage-source converters with grid-forming control: a design-oriented study," *IEEE Journal of Emerging and Selected Topics in Power Electronics*, vol. 8, no. 2, pp. 1019-1033, Jun. 2020.
- [8] C. Li, Y. Yang, Y. Li *et al.*, "Modeling for oscillation propagation with frequency-voltage coupling effect in grid-connected virtual synchronous generator," *IEEE Transactions on Power Electronics*, vol. 40, no. 1, pp. 82-86, Jan. 2025.
- [9] C. Li, Y. Li, Y. Du *et al.*, "Self-stability and induced-stability analysis for frequency and voltage in grid-forming VSG system with generic magnitude-phase model," *IEEE Transactions on Industrial Informatics*, vol. 20, no. 10, pp. 12328-12338, Oct. 2024.
- [10] C. Shen, W. Gu, and W. Liu, "Design-oriented transient stability analysis of virtual synchronous generators under mode-switching frt control," in *Proceedings of 2022 IEEE 5th International Electrical and Energy Conference*, Nanjing, China, May 2022, pp. 147-152.
- [11] C. Luo, Y. Chen, S. Liao *et al.*, "Design-oriented analysis and transient control for VSG with current saturation unit," *IEEE Transactions on Power Electronics*, vol. 40, no. 1, pp. 2472-2483, Jan. 2025.
- [12] T. Qoria, E. Rokrok, A. Bruyere *et al.*, "A PLL-free grid-forming control with decoupled functionalities for high-power transmission system applications," *IEEE Access*, vol. 8, pp. 197363-197378, Oct. 2020.
- [13] J. Girona-Badia, V. A. Lacerda, D. W. Spier *et al.*, "Resource-aware grid-forming synchronization control: design, analysis and validation," *IEEE Transactions on Energy Conversion*, vol. 40, no. 3, pp. 2548-2561, Sept. 2025.
- [14] J. Girona-Badia, E. Prieto-Araujo, and O. Gomis-Bellmunt, "Pairing grid-forming VSC filter topologies with voltage control structures," *International Journal of Electrical Power & Energy Systems*, vol. 155, p. 109670, Jan. 2024.
- [15] S. K. Chung, "A phase tracking system for three phase utility interface inverters," *IEEE Transactions on Power Electronics*, vol. 15, no. 3, pp. 431-438, May 2000.
- [16] J. Girona-Badia, V. A. Lacerda, E. Prieto-Araujo *et al.*, "Limitations on the virtual inertia provision from grid-forming-connected renewable energy sources," *IET Conference Proceedings*, vol. 2023, no. 1, pp. 166-173, Mar. 2023.
- [17] P. Rodríguez, A. Luna, I. Candela *et al.*, "Multiresonant frequency-locked loop for grid synchronization of power converters under distorted grid conditions," *IEEE Transactions on Industrial Electronics*, vol. 58, no. 1, pp. 127-138, Jan. 2011.
- [18] J. A. Suul, S. D'Arco, and G. Guidi, "A single-phase virtual synchronous machine for providing vehicle-to-grid services from electric vehicle battery chargers," in *Proceedings of the International Electric Vehicle Technology Conference & Automotive Power Electronics*, Yokohama, Japan, May 2014, pp. 1-77.
- [19] J. A. Suul, S. D'Arco, and G. Guidi, "Virtual synchronous machine-based control of a single-phase bi-directional battery charger for providing vehicle-to-grid services," *IEEE Transactions on Industry Applications*, vol. 52, no. 4, pp. 3234-3244, Apr. 2016.
- [20] J. Freytes, A. Rossé, V. Costan *et al.* (2023, Mar.). Grid-forming control based on emulated synchronous condenser strategy compliant with challenging grid code requirements. [Online]. Available: <https://www.bohrium.com/paper/2303.00391>
- [21] O. Mo, S. D'Arco, and J. A. Suul, "Evaluation of virtual synchronous machines with dynamic or quasi-stationary machine models," *IEEE Transactions on Industrial Electronics*, vol. 64, no. 7, pp. 5952-5962, Jul. 2017.
- [22] P. Kundur, *Power System Stability and Control*. New York: McGraw-Hill, 1994.

**Jaume Girona-Badia** received the bachelor and master degrees in industrial engineering from the School of Industrial Engineering of Barcelona (ET-SEIB), Barcelona, Spain, in 2020 and 2021, respectively, and the Ph.D. degree in electrical engineering from Universitat Politècnica de Catalunya (UPC), Barcelona, Spain, in 2025. He is currently a Senior Engineer with CITCEA-UPC, Barcelona, Spain. His research interests include the fields linked with power electronics and renewable energy integration in power systems.

**Juan Carlos Olives-Camps** received the bachelor degree in power system engineering from the Universitat Politècnica de Catalunya (UPC), Barcelona, Spain, in 2014, and the master degree in the same field from the University of Seville, Seville, Spain, in 2019. He is currently pursuing the Ph.D. degree in power systems engineering. In 2023, he joined the CITCEA-UPC, Barcelona, Spain. His research interests include control and modeling of power system, and dynamic analysis of system dominated by power electronic converter.

**Vinicius Albernaz Lacerda** received the B.Sc. and Ph.D. degrees in electrical engineering from the University of São Paulo, São Paulo, Brazil, in 2015 and 2021, respectively. From 2018 to 2019 he was a Visiting Researcher with the University of Strathclyde, Glasgow, UK. He joined the Universitat Politècnica de Catalunya (UPC), Barcelona, Spain, in 2021 and he is currently a Lecturer at CITCEA-UPC, Barcelona, Spain. He is currently a Senior Power Systems Engineer at eRoots Analytics. His research interests include electromagnetic transient (EMT) and phasor simulation of modern power grids and control and design of grid-forming converter.

**Eduardo Prieto-Araujo** received the B.Sc. degree in industrial engineering and the Ph.D. degree in electrical engineering from the School of Industrial Engineering of Barcelona, Universitat Politècnica de Catalunya (UPC), Barcelona, Spain, in 2011 and 2016, respectively. He joined CITCEA-UPC, Barcelona, Spain, in 2010. He is currently a Serra Hunter Lecturer with the Electrical Engineering Department, UPC. In 2021, he was a Visiting Professor with the Automatic Control Laboratory, ETH Zürich, Zürich, Switzerland. In 2022, he co-founded the start-up eRoots focused on the analysis of modern power system. His research interests include renewable generation system, control of power converter for high-voltage DC (HVDC) applications, interaction analysis between converters, and power electronics dominated power system.

**Oriol Gomis-Bellmunt** received the B.Sc. degree in industrial engineering and the Ph.D. degree in electrical engineering from the School of Industrial Engineering of Barcelona (ETSEIB), Universitat Politècnica de Catalunya (UPC), Barcelona, Spain, in 2001 and 2007, respectively. In 1999, he joined Engitrol S.L., where he worked as Project Engineer in the automation and control industry. Since 2004, he has been with the Electrical Engineering Department, UPC, where he is a Professor and participates in the CITCEA-UPC, Barcelona, Spain. Since 2020, he is an ICREA Academia Researcher. In 2022, he co-founded the start-up eRoots Analytics focused on the analysis of modern power system. His research interests include power electronics and renewable energy integration in power system.